Buried iceberg-keel scouring on the southern Spitsbergenbanken, NW Barents Sea

Massimo Zecchin[a,*], Michele Rebesco[a], Renata G. Lucchi[a], Mauro Caffau[a], Hendrik Lantzsch[b], Till J.J. Hanebuth[b,c]

[a] OGS (Istituto Nazionale di Oceanografia e di Geofisica Sperimentale), 34010 Sgonico (TS), Italy

[b] MARUM - Center for Marine Environmental Sciences, University of Bremen, 28334 Bremen, Germany

[c] School of Coastal and Marine Systems Science, Coastal Carolina University, Conway, SC 29526, United States of America

*Corresponding author.

E-mail address: mzecchin@ogs.trieste.it (M. Zecchin).

ABSTRACT

PARASOUND (3.5 kHz) subbottom echosounder profiles acquired on the southern Spitsbergenbanken, NW Barents Sea, show iceberg-keel scouring features which are buried by sediment that accumulated during the post Last Glacial Maximum (LGM) sea-level rise. Four acoustic units (Units 1 to 4 in stratigraphic order) were differentiated, based on the characterization of their acoustic facies and reflection surfaces. Unit 1 shows a chaotic internal structure and is interpreted as a glacial till, whereas the laminated Units 2 to 4 accumulated by sediment settling from suspension clouds and bottom currents during the last deglaciation phase. The top of Unit 2 was frequently incised by iceberg keels, resulting in up to 12 m deep ploughmarks which were later filled and buried by Unit 3 and 4 sediments. Three main paleo-evironmental changes controlled the evolution of the facies succession: (1) The major shift from till formation (Unit 1) below grounded ice to the accumulation of laminated sediments (Unit 2) which are inferred to reflect ice lifting and meltwater release; (2) Iceberg-keel scouring after sedimentation of Unit 2; (3) the probable abrupt termination of iceberg-keel scouring related to the glacio-eustatic sea-level rise. A linkage between these episodes of changes and short-lasting phases of rapid post LGM sea-level rise, such as meltwater pulses, is inferred, although further studies are needed to better understand the temporal and genetic relationships between the sedimentary events recognized in the Barents Sea and climate changes.

Keywords: Iceberg-keel scouring; Ploughmarks; Barents Sea; Meltwater pulses; Spitsbergenbanken.

1. Introduction

Ploughmarks related to iceberg-keel scouring and mega-scale glacial lineations are well-known features on high-latitude continental margins, as they are commonly found in both Arctic and Antarctic continental shelf areas and in shelf-margin topographic troughs carved by grounding ice (e.g., Ó Cofaigh et al., 2005; Dowdeswell and Bamber, 2007; López-Martínez et al., 2011; Rebesco et al., 2011; Robinson and Dowdeswell, 2011; Bjarnadóttir et al., 2013; Andreassen et al., 2014). In particular, among shelf-margin troughs, km-long ploughmarks were found in the Kveithola Trough (western Barents Sea Shelf) down to 350 modern water depth on top of grounding zone wedges that accumulated during the last deglacial phase (Rebesco et al., 2011; Bjarnadóttir et al., 2013; Hanebuth et al., 2014). This finding indicates that ploughmarks scoured by the keels of icebergs formed just after the break-up of previously grounded ice, i.e., during the post Last Glacial Maximum (LGM) glacio-eustatic sea-level rise. Ploughmarks can be linear to curvilinear and may exhibit abrupt changes in direction (Dowdeswell et al., 2007; López-Martínez et al., 2011; Rebesco et al., 2011; Andreassen et al., 2014).

Previous studies in the Barents Sea have mapped the seabed morphology and reconstructed glacimarine sedimentary processes during the deglaciation in the Storfjorden and Kveithola Troughs and shelf margins (Pedrosa et al., 2011; Rebesco et al., 2011, 2012, 2014; Lucchi et al., 2012, 2013; Rüther et al., 2013; Andreassen et al., 2014; Bjarnadóttir et al., 2014). The present study aims at illustrating buried iceberg-keel ploughmarks on the southern Spitsbergenbanken, near the northern margin of the Kveithola Trough, by means of PARASOUND subbottom echosounder profiles (Fig. 1). The recognition of buried ploughmarks is uncommon (e.g., Long and Praeg, 1997), and their burial reflects locally abundant sediment supply during the post-LGM glacio-eustatic sea-level rise. The study of sediments burying these erosional features is important, as they likely record main environmental changes and meltwater episodes, helping to improve the knowledge on post-LGM climate changes at high-latitudes.

2. Geological setting

The study area is located in the NW Barents Sea, on the southern part of the Spitsbergenbanken, just NE of the Kveithola Trough (Fig. 1A,B). A rifting phase between Greenland and Spitsbergen, leading to the opening of the Fram Strait, started during the Oligocene, and a narrow oceanic corridor developed during early Miocene (Engen et al., 2008). The Barents Sea, which covers one of the widest continental shelves in the world, is dissected by glacially-carved troughs (e.g. the Bear Island Trough, the Storfjorden and Kveithola Troughs (Andreassen et al., 2004, 2014; Winsborrow et al., 2010; Pedrosa et al., 2011; Rebesco et al., 2011) that are associated with wide trough mouth fans at the continental slope (Fig. 1A,B).

A Plio-Pleistocene progradational phase favored by tectonic uplift and high sediment supply, initially related to fluvial discharge and to subglacial sediment discharge later on, led to the seaward expansion of the shelf margin by up to 150 km and to the formation of the topographic troughs (Forsberg et al., 1999; Dahlgren et al., 2005). An ice sheet covered the northern part of the Barents Sea since the late Pliocene, progressively expanding to the south (Vorren and Laberg, 1997; Knies et al., 2009). The Spitsbergenbanken was covered by a marine-based ice dome during the LGM, whereas paleo-ice streams flowed in the Storfjorden and Kveithola troughs (Lucchi et al., 2013) (Fig. 1A,B). E-W trending mega-scale glacial lineations, recording ice stream movement, developed inside the Kveithola Trough during LGM, and got in parts overprinted by grounding-zone wedges during the early deglaciation (Rebesco et al., 2011; Bjarnadóttir et al., 2013). The huge sediment supply due to an exceptionally large output of glacial meltwater led to the accumulation of relatively thick plumite sequences (*sensu* Hesse et al., 1997) on the Svalbard margin and on the Storfjorden and Kveithola Trough mouth fans during the subsequent later deglaciation phase (Fohrmann et al., 1998; Rasmussen et al., 2007; Jessen et al., 2010; Lucchi et al., 2013; Rasmussen and Thomsen, 2014, 2015; Llopart et al., 2015).

3. Methods

The acoustic profiles used in this study (Fig. 1C) were acquired using a PARASOUND DS III-P70 system (Atlas Hydrographic) during research cruise MSM30 CORIBAR with the German RV

MARIA S. MERIAN in July/August 2013 (Hanebuth et al., 2013). The PARASOUND system generates two primary frequencies (PHF: Primary High Frequency) selectable between 18 and 33 kHz and transmitting in a narrow beam, which allows lower received reverberation levels and, thus, higher penetration. The nonlinear acoustic interaction of the primary frequencies within the water column (Parametric Effect) takes place in the emission cone of these high frequency signals with the aperture angle of 4.5° x 5°. This cone is generated by a rectangular plate of approx. 1 m^2 in size on which there is a transducer array with 128 transducers. Therefore, the beam footprint at the seafloor has a diameter of 7% of the water depth, which inhibits formation of significant diffraction hyperbolas and provides an increased lateral resolution compared to conventional 3.5 kHz subbottom profiling systems.

As a result of the parametric effect, two secondary harmonic frequencies are generated: one parametric signal is the difference (approx. 4 kHz) called Secondary Low Frequency (SLF) and the other parametric signal is the sum of two primary frequencies (approx. 40 kHz) called Secondary High Frequency (SHF). The parametric frequency and 70 kW transmission power allows subbottom penetration up to 200 m (depending on the sediment composition) with a vertical resolution of about 40 cm.

PARASOUND DS III-P70 was controlled by the Atlas Hydromap Control software, which was used to run the system, and Atlas Parastore-3 which has been used for online visualization of received data, data storage, and printing. Parastore-3 has provided also replaying of recorded data, post-processing and further data storage in different output formats (PS3 and/or SEG-Y).

Sedimentological analyses and radiocarbon dating were performed on the 4.42 m-long gravity core GeoB17623-2, collected at 150 m water depth, at 75°0,46’ N, 17°58,85’ E (Fig. 1C). The unopened core was radiographed and analyzed for magnetic susceptibility (k) and wet bulk density at 1 cm resolution. Sediment porosity values were calculated based on electrical conductivity measurements under the assumption of water saturated pore space. The sediment color was determined using the

Munsell soil color charts (Munsell, 1990). Sediment samples were collected at every 10 cm and analyzed for paleontological and petrographic composition. Five horizons were dated through AMS ^{14}C age determination using mixed benthic foraminifera (Table 1). The raw ^{14}C ages were calibrated to calendar-equivalent years using the Calib 7.1 (Stuiver and Reimer, 1993) with the marine13 calibration dataset (Reimer et al., 2013), applying a delta R= 67 ± 34 (Bear Island, Mangerud and Gulliksen, 1975). Calibrated ages are given in ±1 and ±2 sigma ranges and with their median probability value (Table 1) which is, according to Telford et al. (2004), considered the most reliable estimation of a calibrated age.

4. Results

4.1. Acoustic units

Four acoustic units (Unit 1 to Unit 4 from the base to the top) were defined from the PARASOUND profiles based on acoustic facies appearance and bounding internal surfaces (Figs. 2-6 and Table 2).

4.1.1. Unit 1: Opaque, structureless

Unit 1 is found in the whole study area. It exhibits an opaque acoustic facies masking the signal, so that its base is not recognizable in the PARASOUND profiles (Figs. 2-6). The upper boundary of the unit is usually irregular and locally represented by a mounded surface (Figs. 2-6). In places where this boundary is difficult to identify, it is difficult to distinguish between Units 1 and 2. Occasional inclined, low-amplitude internal reflections merge with the upper boundary (Figs. 2-6). The deposit is occasionally dissected by normal faults (Fig. 5).

4.1.2. Unit 2: Semitransparent, chaotic to laminated

Unit 2 is up to ca. 15 m thick and overlies Unit 1. It shows a marked variability in its acoustic character depending on the location. It is mostly chaotic or semitransparent, and exhibits an extremely irregular upper boundary toward the morphological highs; it here, resembles the profile of V- to U-shaped erosional features and more irregular, up to 12 m deep incisions (Figs. 2-6). The chaotic acoustic facies is characterized by the presence of irregularly distributed and variably inclined segments of reflections, in places with a convex shape. These reflections may pass laterally or vertically into irregular areas of variable size having high amplitude, and to more transparent areas without internal reflections (Figs. 2-6). In places the appearance is so irregular that the unit seems to be composed of dismembered rounded blocks. These deposits rapidly grade downdip, toward the adjacent depressions into laminated deposits characterized by medium- to high-amplitude irregularly undulating reflections, which drape the irregular top of Unit 1 (Figs. 3-6). This lateral facies variation typically occurs within just a few hundreds of meters. The laminated facies does not exhibit an incised upper boundary, and it may contain isolated vertically elongated transparent areas (Fig. 5). Rare normal faults with meter-scale displacement dissect the deposit (Fig. 5). Unit 2 is locally exposed at the seafloor in areas where the younger Units 3 and 4 are absent (Figs. 2-6).

4.1.3. Unit 3: Laminated, high-amplitude

Unit 3 shows high-amplitude, sub-horizontal to inclined reflections that onlap the top of Unit 2, levelling the topographic irregularities (Figs. 2-6). Its sediment thickness ranges from zero at some topographic highs to ca. 15 m (Figs. 2-6). The contact between Units 2 and 3 is unconformable and usually characterized by very high-amplitude signals (Figs. 2-6). Where Unit 2 appears well laminated, i.e. inside deeper depressions, the boundary between Unit 2 and Unit 3 may be difficult to identify apparently being conformable (Figs. 3, 4 and 6). The top of Unit 3 is usually undulating, as it follows the irregular underlying topography that has not been completely smoothed (Figs. 2-6). Unit 3 is not dissected by the normal faults affecting Units 1 and 2. Small clinoform bodies are occasionally found near the top of the unit and fill the previously-created fault scarps and other depressions (Fig. 5).

4.1.4. Unit 4: Laminated, low-amplitude

Unit 4 can be distinguished from the underlying Unit 3 by its average lower amplitude which makes its appearance more transparent, except for the topographically low areas where both units appear relatively transparent (Figs. 2-6). The thickness of Unit 4 ranges from zero at some topographic highs to ca. 10 m (Figs. 2-6). Unit 4 is laminated and conformably drapes the boundary between Units 3 and 4 (Figs. 2-6). The reflections of Unit 4 show local onlap or downlap relationships with this boundary (Figs. 2-6). Where Unit 3 is absent, Unit 4 unconformably overlies Unit 2 (Figs. 2-6). Higher amplitude reflections are occasionally found in the lower part of the unit. The top of Unit 4 corresponds with the modern seafloor.

4.2. Core analysis

Profile 20130725_1752 (Fig. 3) intercepts Core GeoB17623-2. Three lithofacies were identified in core GeoB17623-2: a lower muddy facies (Facies A, 4.42-3.15 m below modern seafloor/bsf), an intermediate sandy facies (Facies B, 3.15-1.40 m bsf), and an upper muddy facies (Facies C, 1.40-0 m bsf; Fig. 7).

Facies A consists of faintly laminated quartz silt and silty clay with occasional layers of gravel-sized IRD (*sensu* Grobe, 1987) (Fig. 7). The color is black (5y 2.5/1) in the lower and middle parts, and very dark gray (5y 3/1) in the upper part (Fig. 7). Facies A contains pyritized burrows and polychaete tubes (Fig. 8A), pyrite encrustations (Fig. 8A), and occasional benthic foraminifera (Fig. 8B), ostracods, mollusc fragments, bryozoans and fish vertebrae. The lamination is planar and laterally continuous although not very evident, especially in the upper part of the facies, where a sharp, oblique surface overlain by shell debris separates Facies A from Facies B (Fig. 7). Facies B is composed of crudely layered (cm-scale), medium- to fine-grained quartz sand showing overall normal grading (Fig. 7). The color is very dark olive gray (5y 3/2) in the lower part, and dark gray (5y 4/1) in the middle and upper parts (Fig. 7). Facies B contains local shell debris and isolated large broken shells, as well as commonly to abundantly benthic foraminifera (Fig. 8C), ostracods, bryozoans, and rarely fish vertebrae. Due to the normal grading, the boundary with Facies C appears gradual (Fig. 7). Facies C consists of bioturbated quartz silt and sand and shell debris (Fig. 7). The color is dark gray (5y 4/1) in the lower and middle parts, and very dark gray (5y 3/1) in the upper part (Fig. 7). Facies C also contains abundantly hyaline and agglutinating benthic foraminifera (Fig. 8D), ostracods, bryozoans, and rarely spines of echinoids and fish vertebrae. Worm tubes are found towards the top of the core.

An overall upward decrease in the inorganic fraction and an increase in the organic fraction are observed in the core. Based on the AMS ^{14}C dating, the boundary that separates Facies A from Facies B has an age between 9,450 and 9,020 cal. years BP, whereas the boundary between Facies B and C dates to 5,860 and 3,410 cal. years BP (Fig. 7 and Table 1).

A comparison between core GeoB17623-2 and the profile 20130725_1752 suggests that the sharp boundary separating Facies A and B from each other corresponds to the marked boundary between Units 3 and 4 (Figs. 3 and 7). The formation of Unit 3, therefore, probably ended at about 9 cal. ka BP, and was subsequently followed by the accumulation of Unit 4.

The porosity exhibits an overall slight decrease from the top of the core to its base, with minor variations (Fig. 7). In contrast, the magnetic susceptibility shows higher values, with superposed minor variations, corresponding to Facies A, and a marked decrease just at the sharp boundary between Facies A and B (Fig. 7). The density increases gradually down to 1 m from the top of the core, and shows an overall modest downward decrease in Facies A (Fig. 7).

4.3. Interpretation of acoustic and core data

The characteristics of Unit 1 resemble those described for till deposits related to grounded ice (e.g., Batchelor et al., 2011; Rebesco et al., 2011; Ó Cofaigh et al., 2005). This fact, together with the stratigraphic position of Unit 1 in the lower part of the sedimentary succession, suggests that this unit is subglacial till, having possibly accumulated during stillstand in grounding-zone position (e.g., Rebesco et al., 2011). The low-amplitude internal reflections within Unit 1 probably represent interfaces between depositional stages having accumulated either during subsequent phases of ice advance or during episodic stillstands at the grounding zone of the ice margin within a recessional trend (Ó Cofaigh et al., 2005; Rebesco et al., 2011; Bjarnadóttir et al., 2013).

The extremely irregular upper boundary of Unit 2 is very similar to the indented surface of deposits that underwent iceberg-keel scouring which produced ploughmarks, as found in both Arctic and Antarctic settings (Dowdeswell et al., 1993; Barnes, 1997; MacLean, 1997; Solheim, 1997; López-Martínez et al., 2011; Robinson and Dowdeswell, 2011). Taking this observation, and the observed lateral transition from a chaotic into a laminated acoustic facies toward the topographic depressions into account, Unit 2 was probably overprinted by iceberg-keel scouring. In particular, this scouring by iceberg keels probably led to the dismembering of the laminated deposits of Unit 2 and to a formation of ploughmarks on the topographic highs, which were later on buried by Units 3 and 4 (Figs. 2-6). In contrast, iceberg keels were probably not deep enough to affect the sediment accumulated inside the topographic depressions. The draping of Unit 2 on Unit 1 is probably the result of the vertical settlement of muddy and sandy sediment during the onset of the deglaciation, originating from hyperpycnal flows (e.g., Rebesco et al., 2011; Lucchi et al., 2013).

The characteristics and position in the sedimentary succession of Units 3 and 4 resemble the features of the laminated Units 1 and 2 identified by Rebesco et al. (2011) inside the adjacent Kveithola Trough, which have been interpreted as the result of hemipelagic settling from suspension, once grounded ice had retreated from this part of the shelf. The succession forming Units 3 and 4, reaching a thickness of ca. 25 m inside topographic lows (Fig. 6), is inferred to be the result of both sediment bedload transport and suspended load having originated from sediment-rich plumes (e.g., Hesse et al., 1997; Lucchi et al., 2013). In particular, on the basis of the analysis of core GeoB17623-2, Unit 3 is thought to have accumulated mainly from suspension clouds related to ice melting carrying muddy sediment. This environment was, in addition, characterized by occasional fall-out of IRD, as documented in Facies A (Fig. 7). As IRD commonly forms distinct layers (Lucchi et al., 2013), the presence of this material explains the higher amplitude of the internal reflections in Unit 3 compared to those in Unit 4. Unit 4 mostly records sediment accumulation from progressively less competent currents forming normally graded successions, as found in Facies B (Fig. 7). The silty to sandy bioturbated deposit of Facies C (i.e., the upper part of Unit 4) is reconcilable with an accumulation controlled by bottom currents (Fig. 7). Moreover, the latest acoustic units in the inner part of the adjacent Kveithola Trough (Rebesco et al., 2016) and on downstream sectors of the continental slope (Rebesco et al., 2013) are interpreted as sediment deposited by bottom currents. Unfortunately, a direct correlation of these units with Unit 4 in our study area is prevented on the steep northern flank of the Kveithola Trough, where sediment accumulation is virtually absent. Nevertheless, on the basis of the sedimentary characteristics of Facies C and the proximity with other bottom current-controlled deposits, we interpret Unit 4 as the result of similar processes (e.g., Rebesco et al., 2014). The marked decrease in magnetic susceptibility just at the sharp boundary between Facies A and B in core GeoB17623-2 (Fig. 7) is probably linked to a higher amount of heavy minerals in the muddy sediments building up Facies A. This switch implies a change in sediment source area at the boundary of Unit 3 and Unit 4. The similarity in acoustic facies appearance of Units 3 and 4 inside low-lying areas suggests a comparable sediment composition at those locations, possibly under the influence of weak bottom currents. The occurrence of small clinoform bodies within Unit 3 is probably the result of local gravity flows related of gradients inside topographic depressions.

5. Discussion

Buried iceberg-keel ploughmarks, similar to those affecting the top of Unit 2 (Figs. 2-6), are uncommon features, as they are usually found exposed on the seafloor inside high-latitude shelf-margin troughs (e.g., Ó Cofaigh et al., 2005; Rebesco et al., 2011; Bjarnadóttir et al., 2013), in high-latitude flatter shelf areas (e.g., Dowdeswell and Bamber, 2007; López-Martínez et al., 2011; Robinson and Dowdeswell, 2011; Andreassen et al., 2014) and straits (Metz et al., 2008). Buried iceberg-keel ploughmarks were described from the Norwegian Sea by Long and Praeg (1997) and in early Quaternary sediments of the North Sea by Dowdeswell and Ottesen (2013). Buried mega-scale glacial lineations have an appearance similar to that of iceberg-keel ploughmarks, but since they are linked to flowing grounded ice they occur at a different stratigraphic position: they affect the top of the basal glacial till rather than the top of the overlying laminated deposits (e.g., Dowdeswell et al., 2014). Tunnel valleys are other erosional features that may be similarly shaped as iceberg-keel ploughmarks (Kristensen et al., 2007). The sediments that are incised by tunnel valleys are, however, not disturbed as it is the case in Unit 2 at the topographic highs, but exhibit the original stratified appearance. In fact, it is the lateral transition from chaotic to laminated acoustic facies into the topographic depressions that provides the strongest indication for iceberg-keel scouring.

Although ages for the deepest part of the succession are not available, the absence of glacial till above Unit 1 suggests that the accumulation of Units 2-4 occurred during the post-LGM glacio-eustatic sea-level rise. In particular, we envisage the following succession of events:

1) After the accumulation of the glacial till during LGM or during ice retreat characterizing the initial post-glacial phase, forming Unit 1 (Fig. 9A), both ice lifting and the flow of meltwater under the ice led to the accumulation of Unit 2 (Fig. 9B). 2) The subsequent phase was characterized by ice break up that produced large icebergs, the keels of which disturbed the sediment that composes Unit 2 on the topographic highs and produced the ploughmarks (Fig. 9C). 3) The large supply of sediment in the area favored by continuous ice melting led to the accumulation of the plumites with

IRD composing Unit 3, which filled the ploughmarks and smoothed the topography of the seafloor (Fig. 9D). During this phase, icebergs have not scoured the seafloor in the study area, as their size has decreased and/or sea level has risen, and therefore iceberg keels were not deep enough to scour the topographic highs (Fig. 9D). 4) The most recent phase, probably concomitant with iceberg free conditions, was characterized by the accumulation of Unit 4 sediments from bottom currents (Fig. 9E). As recent drift deposits were previously found mainly in the eastern, inner part of the Kveithola Trough (Bjarnadóttir et al., 2013; Rebesco et al., 2016), the composite sediment drape recognized on top of grounding-zone wedges in the outer part of the same trough by Rebesco et al. (2011) probably correlates with Units 2 and 3 of the present study. A direct correlation is prevented by the steepness of the slope of Kveithola Trough (where sediment is extremely reduced and virtually absent).

During deposition of the succession, three main episodes can be highlighted: (1) the change from subglacial till deposition toward hyperpycnal sedimentation after the formation of Unit 1 (Fig. 9A,B); (2) iceberg-keel scouring after deposition of Unit 2 (Fig. 9C); (3) the probable abrupt termination of the iceberg-keel scouring (Fig. 9D). One possibility is that both ice lifting between the formation of Units 1 and 2, and the termination of iceberg-keel scouring before Unit 3 started to form, were relatively abrupt events linked to brief episodes of glacio-eustatic sea-level rise usually called meltwater pulses (MWP; Bard et al., 1990; Deschamps et al., 2012). In particular, during MWP 1A (14.6 to 13.5 cal ka BP) the sea level is inferred to have risen from 104-95 to 88-75 m below present sea level in a few centuries (Hanebuth et al., 2000; Deschamps et al., 2012). The phases following both ice-shelf lifting and iceberg-keel scouring in the study area were accompanied respectively by the deposition of Units 2 and 3, which could reflect phases of exceptional glacial meltwater accompanied by rising sea-level and sea surface temperature (e.g., Lucchi et al., 2013, 2015). Following this hypothesis, the sedimentation of Unit 1 would have preceded MWP 1A, whereas Unit 2 would have accumulated after MWP 1A (ca. 14.6 cal ka BP) until sometime between MWP 1A and the Younger Drias stadial (i.e., during the Bølling interstadial), when icebergs started to scour the seafloor. Ice break up leading to the formation of the icebergs may have been the result of combined atmospheric and water warming, irrespective of glacio-eustatic sea-level rise (e.g., Yokoyama et al., 2016). Unit 3 would have accumulated at the onset of a phase of acceleration in sea level rise following the Younger Drias (Fig. 9). The change of sedimentation between Units 3 and 4, dated at ca. 9 cal. ka BP (Fig. 7), is in agreement with such a sea-level related model, and it has marked the onset of the recent iceberg-free Holocene sedimentation. These considerations fit with the conclusions by Jessen et al. (2010) for the western Svalbard continental slope, who noted the onset of accumulation of laminated sediments from meltwater plumes during the Bølling interstadial, just after MWP 1A, and the end of accumulation of IRD-rich sediments at ca. 10 cal ka BP.

From a sequence stratigraphic point of view, the succession is difficult to interpret due to the limited extent of the study area, which represents only a small part of the Barents shelf (Fig. 1). Nevertheless, following the sequence stratigraphic model for high-latitude settings developed by Zecchin et al. (2015), the late Pleistocene to Holocene deposits having accumulated in the inner part of the Kveithola Trough and on the adjacent banks are likely transgressive. In fact, glacigenic deposits accumulated during ice advance and LGM are likely reworked and incorporated into backstepping moraines and grounding zone wedges, bounded below by a Glacial Retreat Surface (GRS), during ice retreat (Bjarnadóttir et al., 2013; Zecchin et al., 2015). The recognized interfaces in Unit 1 might represent lower-rank GRSs which usually merge into a basal GRS (Zecchin et al., 2015) (Fig. 10). Unit 1 is therefore interpreted as the lower part of the transgressive systems tract (TST) of the post-LGM sequence, whereas the overlying Units 2-4 are inferred to mainly represent the upper part of the TST (Fig. 10). Highstand sediments possibly compose the upper part of Unit 4 (Fig. 10).

6. Conclusions

High-resolution PARASOUND subbottom echosounder data collected at the southern margin of the Spitsbergenbanken document sedimentation interpreted to be related to post-LGM ice shelf melting. In particular, the following general conclusions can be made:

- The depositional-erosional succession is composed of four units (Units 1 to 4 from base to top), defined on the basis of acoustic facies characterization and bounding surfaces. Unit 1 is interpreted as a glacial till, whereas Units 2 to 4 record sedimentation from suspension clouds and bottom currents during the deglaciation phase. Unit 2 got strongly disturbed by iceberg keels on local topographic highs, leaving up to 12 m deep ploughmarks subsequently buried by the deposits of the overlying Units 3 and 4.
- Three main episodes can be highlighted: (1) the change from till sedimentation (Unit 1) below grounded ice to the accumulation of laminated sediments (Unit 2), inferred to reflect ice shelf lifting and meltwater release; (2) iceberg-keel scouring after the formation of Unit 2; (3) the abrupt termination of iceberg-keel scouring possibly related to glacio-eustatic sea-level rise.
- Further research is needed to correlate the sedimentary events found on the Spitsbergenbanken, inside the adjacent troughs and at the neighboring slope areas, with the global eustatic changes known from the middle and lower latitudes. This approach is crucial to detect the local response of glaciated, high-latitude marine areas to large-scale climatic events.

Acknowledgements

CORIBAR research cruise MSM110 was partially funded by the MARUM DFG-Research Center/Cluster of Excellence “The Ocean in the Earth System” as part of MARUM project SD-2, and co-funded by the Italian PNRA-CORIBAR-IT project (PdR 2013/C2.01), the Research Council of Norway through its Centres of Excellence funding scheme (project number 223259), the Spanish MEC project CORIBAR-ES (CTM2011-14807-E), and the Dansk Center for Havforskning, project number 2014_04. Core analyses were supported by the PNRA projects CORIBAR-IT and VALFLU, the Spanish MEC project DEGLABAR (CTM2010-17386), and the ARCA project (grant n. 25_11_2013_973). We acknowledge the scientific party of CORIBAR cruise and project, and R. Romeo for core logging. This study contributes to the IPY initiative 367 NICESTREAM (Neogene Ice Streams and Sedimentary Processes on High- Latitude Continental Margins).

References

Andreassen, K., L.C. Nilssen, B. Rafaelsen and L. Kuilman. 2004. Three-dimensional seismic data from the Barents Sea margin reveal evidence of past ice streams and their dynamics. Geology, 32(8), 729–732.

Andreassen, K., Winsborrow, M.C.M., Bjarnadóttir, L.R., Rüther, D.C., 2014. Document Ice stream retreat dynamics inferred from an assemblage of landforms in the northern Barents Sea. Quaternary Science Reviews 92, 246-257.

Andreassen, K., Winsborrow, M.C.M., Bjarnadóttir, L.R., Rüther, D.C., 2014. Ice stream retreat dynamics inferred from an assemblage of landforms in the northern Barents Sea. Quaternary Science Reviews 92, 246-257.

Bard, E., Hamelin, B., Fairbanks, R.G., 1990. U-Th ages obtained by mass spectrometry in corals from Barbados: sea level during the past 130,000 years. Nature 346, 456-458.

Barnes, P.W., 1997. Iceberg gouges on the Antarctic shelf. In: Davies, T.A., Bell, T., Cooper, A.K., Josenhans, H., Polyak, L., Solheim, A., Stoker, M.R., Stravers, J.A. (Eds.), Glaciated Continental Margins: An Atlas of Acoustic Images. Chapman & Hall, London, pp. 154-155.

Batchelor, C.L., Dowdeswell, J.A., Hogan, K.A., 2011. Late Quaternary ice flow and sediment delivery through Hinlopen Trough, Northern Svalbard margin: Submarine landforms and depositional fan. Marine Geology 284, 13-27.

Bjarnadóttir, L.R., Rüther, D.C., Winsborrow, M.C.M., Andreassen, K., 2013. Grounding-line dynamics during the last deglaciation of Kveithola, W Barents Sea, as revealed by seabed geomorphology and shallow seismic stratigraphy. Boreas 42, 84-107.

Bjarnadóttir, L.R., Winsborrow, M.C.M., Andreassen, K., 2014. Deglaciation of the central Barents Sea. Quaternary Science Reviews 92, 208-226.

Dahlgren, K.I.T., Vorren, T.O., Stoker, M.S., Nielsen, T., Nygård, A., Sejrup, H.P., 2005. Late Cenozoic Prograding wedges on the NW European continental margin: their formation and relationship to tectonics and climate. Marine and Petroleum Geology 22, 9-10.

Deschamps, P., Durand, N., Bard, E., Hamelin, B., Camoin, G., Thomas, A.L., Henderson, G.M., Okuno, J., Yokoyama, Y., 2012. Ice-sheet collapse and sea-level rise at the Bølling warming 14,600 years ago. Nature 483, 559-564.

Dowdeswell, J.A., Bamber, J.L., 2007. Keel depths of modern Antarctic icebergs and implications for sea-floor scouring in the geological record. Marine Geology 243, 120-131.

Dowdeswell, J.A., Hogan, K.A., O´ Cofaigh, C., Fugelli, E.M.C., Evans, J., Noormets, R., 2014. Late Quaternary ice flow in a West Greenland fjord and cross-shelf trough system: submarine landforms from Rink Isbrae to Uummannaq shelf and slope. Quaternary Science Reviews 92, 292-309.

Dowdeswell, J.A., Ottesen, D., 2013. Buried iceberg ploughmarks in the early Quaternary sediments of the central North Sea: A two-million year record of glacial influence from 3D seismic data. Marine Geology 344, 1-9.

Dowdeswell, J.A., Ottesen, D., Rise, L., Craig, J., 2007. Identification and preservation of landforms diagnostic of past ice-sheet activity on continental shelves from three-dimensional seismic evidence. Geology 35, 359-362.

Dowdeswell, J.A., Villinger, H., Whittington, R.J., Marienfeld, P., 1993. Iceberg scouring in Scoresby Sund and on the East Greenland continental shelf. Marine Geology 111, 37-53.

Engen, Ø., Faleide, J.I., Dyreng, T.K., 2008. Opening of the Fram Strait gateway: A review of plate tectonic constraints. Tectonophysics 450, 51-69.

Fohrmann, H., Backhaus, J.O., Blaume, F., Rumohr, J., 1998. Sediments in bottom-arrested gravity plumes: Numerical case studies. J Phys Oceanogr. 28, 2250-2274.

Forsberg, C.F., Solheim, A., Elverhøi, A., Jansen, E., Channell, J.E.T., 1999. The depositional environment of the western Svalbard margin during the Pliocene and the Pleistocene: Sedimentary facies changes at Site 986. Proceedings of the Ocean Drilling Program, Scientific Results 162, 233-246.

Grobe, 1987. A simple method for the determination of ice-rafted debris in sediment cores. Polarforschung 57, 123-126.

Hanebuth, T.J.J., Bergenthal, M., Caburlotto, A., Dippold, S., Düßmann, R., Freudenthal, T., Hörner, T., Kaszemeik, K., Klar, S., Lantzsch, H., Llopart, J., Lucchi, R.G., Nicolaisen, L.S., Noorlander, K., Osti, G., Özmaral, A., Rebesco, M., Rosiak, U., Sabbatini, A., Schmidt, W., Stachowski, A., Urgeles, R., 2013. CORIBAR - Ice dynamics and meltwater deposits: coring in the Kveithola Trough, NW Barents Sea, RV MARIA S. MERIAN cruise MSM30, July 16 – Aug 15, 2013, Tromsø (Norway) – Tromsø (Norway). Berichte, MARUM Zentrum für Marine Umweltwissenschaften, Fachbereich Geowissenschaften, Universität Bremen, 299, 74 pp., Bremen 2013, ISSN 2195-7894.

Hanebuth, T.J.J., Rebesco, M., Urgeles, R., Lucchi, R.G., Freudenthal, T., 2014. Drilling glacial deposits in offshore polar regions. Eos 95 (31), 277-278.

Hesse, R., Khodabakhsh, S., Klauck, I., Ryan, W.B.F., 1997. Asymmetrical turbid surface-plume deposition near ice-outlets of the Pleistocene Laurentide ice sheet in the Labrador Sea. Geo-Marine Letters 17, 179-187.

Jakobsson, M., Mayer, L., Coakley, B., Dowdeswell, J.A., Forbes, S., Fridman, B., Hodnesdal, H., Noormets, R., Pedersen, R., Rebesco, M., Schenke, H.W., Zarayskaya, Y., Accettella, D., Armstrong, A., Anderson, R.M., Bienhoff, P., Camerlenghi, A., Church, I., Edwards, M., Gardner, J.V., Hall, J.K., Hell, B., Hestvik, O., Kristoffersen, Y., Marcussen, C., Mohammad, R., Mosher, D., Nghiem, S.V., Pedrosa, M.T., Travaglini, P.G., Weatherall, P. 2012. The International Bathymetric Chart of the Arctic Ocean (IBCAO) Version 3.0. Geophysical

Research Letters 39, L12609.
Jessen, S.P., Rasmussen, T.L., Nielsen, T., Solheim, A., 2010. A new Late Weichselian and Holocene marine chronology for the western Svalbard slope 30,000-0 cal years BP. Quaternary Science Reviews 29, 1301-1312.
Knies, J., Matthiessen, J., Vogt, C., Laberg, J.S., Hjelstuem, B.O., Smelror, M., Larsen, E., Andreassen, K., Eidvin, T., Vorren, T.O., 2009. The Plio-Pleistocene glaciations of the Barents Sea-Svalbard region: a new model based on revised chronostratigraphy. Quaternary Science Reviews 28, 812-829.
Kristensen, T.B., Huuse, M., Piotrowski, J.A., Clausen, O.R., 2007. A morphometric analysis of tunnel valleys in the eastern North Sea based on 3D seismic data. Journal of Quaternary Science 22, 801-815.
Llopart J., Urgeles R., Camerlenghi A., Lucchi R., Rebesco M., De Mol B., 2015. Late Quaternary development of the Storfjorden and Kveithola Trough Mouth Fans, northwestern Barents Sea. Quaternary Science Reviews 129, 68-84.
Long, D., Praeg, D., 1997. Buried ice-scours: 2D vs 3D-seismic geomorphology. In: Davies, T.A., Bell, T., Cooper, A.K., Josenhans, H., Polyak, L., Solheim, A., Stoker, M.R., Stravers, J.A. (Eds.), Glaciated Continental Margins: An Atlas of Acoustic Images. Chapman & Hall, London, pp. 142-143.
López-Martínez, J., Muñoz, A., Dowdeswell, J.A., Linés, C., Acosta, J., 2011. Relict sea-floor ploughmarks record deep-keeled Antarctic icebergs to 45°S on the Argentine margin. Marine Geology 288, 43-48.
Lucchi, R.G., Pedrosa, M.T., Camerlenghi, A., Urgeles, R., De Mol, B., Rebesco, M., 2012. Recent submarine landslides on the continental slope of Storfjorden and Kveithola trough-mouth fans (north west Barents Sea). In: Yamada, Y., Kawamura, K., Ikehara, K., Ogawa, Y., Urgeles, R., Mosher, D., Chaytor, J., Strasser, M. (Eds.), Submarine Mass Movements and Their Consequences. Advances in Natural and Technological Hazards Research 31, p. 735-745. Springer, Berlin.
Lucchi, R.G., Camerlenghi, A., Rebesco, M., Colmenero-Hidalgo, E., Sierro, F.J., Sagnotti, L., Urgeles, R., Melis, R., Morigi, C., Bárcena, M.-A., Giorgetti, G., Villa, G., Persico, D., Flores, J.-A., Rigual-Hernández, A.S., Pedrosa, M.T., Macri, P., Caburlotto, A., 2013. Postglacial sedimentary processes on the Storfjorden and Kveithola trough mouth fans: Significance of extreme glacimarine sedimentation. Global and Planetary Change 111, 309-326.
Lucchi, R.G., Sagnotti, L., Camerlenghi, A., Macrì, P., Rebesco, M., Pedrosa, M.T., and Giorgetti, G., 2015. Marine sedimentary record of Meltwater Pulse 1a along the NW Barents Sea continental margin. Arktos, 1-7. http://dx.doi.org/10.1007/s41063-015-0008-6
MacLean, B., 1997. Iceberg turbate on southeastern Baffin Island shelf, Canada. In: Davies, T.A., Bell, T., Cooper, A.K., Josenhans, H., Polyak, L., Solheim, A., Stoker, M.R., Stravers, J.A. (Eds.), Glaciated Continental Margins: An Atlas of Acoustic Images. Chapman & Hall, London, pp. 144-145.

Mangerud, J., Gulliksen, S., 1975. Apparent radiocarbon ages of recent marine shells from Norway, Spitsbergen, and Arctic Canada. Quaternary Research 5, 263-273.

Metz, J.M., Dowdeswell, J.A., Woodworth-Lynas, C.M.T., 2008. Sea-floor scour at the mouth of Hudson Strait by deep-keeled icebergs from the Laurentide Ice Sheet. Marine Geology 253, 149-159.

Munsell, 1990. Munsell soil color charts. Koll Morgen Instruments Corporation, Maryland.

O´ Cofaigh, C., Dowdeswell, J.A., Allen, C.S., Hiemstra, J.F., Pudsey, C.J., Evans, J., Evans, D.J.A., 2005. Flow dynamics and till genesis associated with a marine-based Antarctic palaeo-ice stream. Quaternary Science Reviews 24, 709-740.

Rasmussen, T.L., Thomsen, E., Ślubowska, M.A., Jessen, S., Solheim, A., Koç, N., 2007. Paleoceanographic evolution of the SW Svalbard margin (76°N) since 20,000 ^{14}C yr BP. Quaternary Research 67, 100-114.

Rasmussen, T.L., Thomsen, E., 2014. Brine formation in relation to climate changes and ice retreat during the last 15,000years in Storfjorden, Svalbard, 76-78N. Paleoceanography 29, 911–929.

Rasmussen, T.L., Thomsen, E., 2015. Palaeoceanographic development in Storfjorden, Svalbard, during the deglaciation and Holocene: Evidence from benthic foraminiferal records. Boreas 44, 24–44.

Rebesco, M., Liu, Y., Camerlenghi, A., Winsborrow, M., Laberg, J.S., Caburlotto, A., Diviacco, P., Accettella, D., Sauli, C., Wardell, N., Tomini, I., 2011. Deglaciation of the western margin of the Barents Sea Ice Sheet - A swath bathymetric and sub-bottom seismic study from the Kveithola Trough. Marine Geology 279, 141-147.

Rebesco, M., Laberg, J.S., Pedrosa, M.T., Camerlenghi, A., Lucchi, R.G., Zgur, F., Wardell, N., 2014. Onset and growth of Trough-Mouth Fans on the North-Western Barents Sea margin – implications for the evolution of the Barents Sea/Svalbard Ice Sheet. Quaternary Science Reviews 92, 227-234.

Rebesco, M., Pedrosa, M.T., Camerlenghi, A., Lucchi, R.G., Sauli, C., De Mol, B., Madrussani, G., Urgeles, R., Rossi, G., Böhm, G., 2012. One million years of climatic generated landslide events on the northwestern Barents Sea continental margin. In: Yamada, Y., Kawamura, K., Ikehara, K., Ogawa, Y., Urgeles, R., Mosher, D., Chaytor, J., Strasser, M. (Eds.), Submarine Mass Movements and Their Consequences. Advances in Natural and Technological Hazards Research 31, p. 747-756. Springer, Berlin.

Rebesco, M., Wahlin, A., Laberg, J.S., Schauer, U., Beszczynska-Möller, A., Lucchi, R.G., Noormets, R., Accettella, D., Zarayskaya, Y., Diviacco, P., 2013. Quaternary contourite drifts of the Western Spitsbergen margin. Deep-Sea Research I 79, 156-168.

Rebesco, M., Hernández Molina J., van Rooij, D., Wåhlin, A., 2014. Contourites and associated sediments controlled by deep-water circulation processes: state-of-the-art and future considerations. Marine Geology 352, 111-154.

Rebesco M., Özmaral A., Urgeles R., Accettella D., Lucchi R., Rüther D., Winsborrow M., Llopart J., Caburlotto A., Lantzsch H., Hanebuth T.J., 2016. Evolution of a high-latitude sediment drift inside a glacially-carved trough based on high-resolution seismic stratigraphy (Kveithola, NW Barents Sea). Quaternary Science Reviews 147, 178-193.

Rebesco M., Urgeles R., Özmaral A., Coribar Scientific Party, in press. Grounding Zone Wedges, Kveithola Trough (NW Barents Sea). In: Dowdeswell, J.A., Canals, M., Jakobsson, M., Todd, B.J., Dowdeswell, E.K., Hogan, K.A. (Eds.), Atlas of Submarine Glacial Landforms. Geological Society of London Memoir.

Reimer, P.J., Bard, E., Bayliss, A., Beck, J.W., Blackwell, P.G., Bronk Ramsey, C., Buck, C.E., Cheng, H., Edwards, R.L., Friedrich, M., Grootes, P.M., Guilderson, T.P., Haflidason, H., Hajdas, I., Hatté, C., Heaton, T.J., Hogg, A.G., Hughen, K.A., Kaiser, K.F., Kromer, B., Manning, S.W., Niu, M., Reimer, R.W., Richards, D.A., Scott, E.M., Southon, J.R., Turney, C.S.M., van der Plicht, J., 2013. IntCal13 and MARINE13 radiocarbon age calibration curves 0-50000 years cal BP. Radiocarbon 55, 1869-1887. DOI: 10.2458/azu_js_rc.55.16947.

Robinson, P., Dowdeswell, J.A., 2011. Submarine landforms and the behavior of a surging ice cap since the last glacial maximum: The open-marine setting of eastern Austfonna, Svalbard. Marine Geology 286, 82-94.

Rüther, D.C., Andreassen, K., Spagnolo, M., 2013. Aligned glaciotectonic rafts on the central Barents Sea seafloor revealing extensive glacitectonic erosion during the last deglaciation. Geophysical Research Letters 40, 6351-6355.

Solheim, A., 1997. Depth-dependent iceberg plough marks in the Barents Sea. In: Davies, T.A., Bell, T., Cooper, A.K., Josenhans, H., Polyak, L., Solheim, A., Stoker, M.R., Stravers, J.A. (Eds.), Glaciated Continental Margins: An Atlas of Acoustic Images. Chapman & Hall, London, pp. 138-139.

Stuiver, M., Reimer, P.J., 1993. Extended 14C database and revised CALIB radiocarbon calibration program. Radiocarbon 35, 215-230.

Telford, R.J., Heegaard, E., Birks, H.J.B., 2004. The intercept is a poor estimate of a calibrated radiocarbon age. The Holocene 14, 296-298.

Vorren, T.O., Laberg, J.S., 1997. Trough mouth fans-palaeoclimate and ice-sheet monitors. Quaternary Science Reviews 16, 865-881.

Winsborrow, M.C.M., Andreassen, K., Corner, G.D., Laberg, J.S., 2010. Deglaciation of a marine-based ice sheet: Late Weichselian palaeo-ice dynamics and retreat in the southern Barents Sea reconstructed from onshore and offshore glacial geomorphology. Quaternary Science Reviews 29, 424-442.

Yokoyama, Y., Anderson, J.B., Yamane, M., Simkins, L.M., Miyairi, Y., Yamazaki, T., Koizumi, M., Suga, H., Kusahara, K., Prothro, L., Hasumi, H., Southon, J.R., Ohkouchi, N., 2016. Widespread collapse of the Ross Ice Shelf during the late Holocene. PNAS 113, 2354-2359.

Zecchin, M., Catuneanu, O., Rebesco, M., 2015. High-resolution sequence stratigraphy of clastic shelves IV: High-latitude settings. Marine and Petroleum Geology 68, 427-437.

FIGURE CAPTIONS

Fig. 1. (A) Location map with the study area (red box) in the NW Barents Sea (bathymetry from IBCAO, Jakobsson et al., 2012). (B) Shaded relief map of the study area, showing the Kveithola Trough and the SW margin of the Spitsbergenbanken (bathymetry from IBCAO with superimposed available mutibeam data, modified from Rebesco et al., 2016). (C) Detail of (B) showing the position of the PARASOUND profiles and core GeoB17623-2.

Fig. 2. PARASOUND profile 20130725_1352 (see Fig. 1C for location). Four acoustic units (Units 1-4) are identified (see the line drawing below). Note the irregular incisions one top of Unit 2, interpreted as iceberg-keel ploughmarks filled by Unit 3 deposits. The main characteristics of the acoustic facies are indicated in the raw profile.

Fig. 3. PARASOUND profile 20130725_1752 and the position of core GeoB17623-2 (see Fig. 1C for location). Four acoustic units (Units 1-4) are identified (see the line drawing below). Note the irregular incisions on top of Unit 2 at the topographic high to the right, interpreted as iceberg-keel ploughmarks filled by Unit 3 deposits. The main characteristics of the acoustic facies are indicated in the raw profile.

Fig. 4. PARASOUND profile 20130724_1405 (segment 1) (see Fig. 1C for location). Four acoustic units (Units 1-4) are identified (see the line drawing below). Note the irregular incisions on top of Unit 2 at the topographic high to the right, interpreted as iceberg-keel ploughmarks filled by Unit 3 deposits. The main characteristics of the acoustic facies are indicated in the raw profile.

Fig. 5. PARASOUND profile 20130724_1405 (segment 2) (see Fig. 1C for location). Four acoustic units (Units 1-4) are identified (see the line drawing below). Note the irregular incisions on top of

Unit 2 at the topographic highs, interpreted as iceberg-keel ploughmarks filled by Unit 3 deposits. Note also the normal fault that dissected both Units 1 and 2. The main characteristics of the acoustic facies are indicated in the raw profile.

Fig. 6. PARASOUND profile 20130804_0034 (see Fig. 1C for location). Four acoustic units (Units 1-4) are identified (see the line drawing below). Note the irregular incisions on top of Unit 2 at the topographic high to the left, interpreted as iceberg-keel ploughmarks filled by Unit 3 deposits. The main characteristics of the acoustic facies are indicated in the raw profile.

Fig. 7. Photograph, X-rays and lithological log of core GeoB17623-2 (see Figs. 1C and 3 for location). The magnetic susceptibility, wet bulk density and porosity are plotted on the right. Calibrated radiocarbon ages are indicated in red on the left. The core succession, composed of three sedimentary facies (Facies A, B and C) covers the whole Unit 4 and the upper part of Unit 3 (see Fig. 3).

Fig. 8. Microphotographs of samples collected in core GeoB17623-2 (see Figs. 1C and 3 for location). (A) Pyrite in the lower part of Facies A (400 cm from the top). (B) Benthic foraminifera in the upper part of Facies A (320 cm from the top). (C) Benthic foraminifera in Facies B (240 cm from the top). (D) Benthic foraminifera in Facies C (40 cm from the top). Abbreviations: a – *Cibicides lobatulus* (ventral view); a1 – *Cibicides lobatulus* (spiral view); b – *Nonionellina labradorica*; c – *Islandiella norcrossi*; d – *Elphidium excavatum*; e – *Cassidulina reniforme*; f – *Cribrostomoides crassimargo*; g – *Reophax difflugiformis*; pb – pyritized burrow; pe – pyritized encrustation; pt – pyritized polychaete tube.

Fig. 9. Interpreted depositional history of Units 1-4. (A) The phase between Last Glacial Maximum

and initial deglaciation was characterized by the accumulation of glacial till at the base of ice shelf (Unit 1). (B) The subsequent sea-level rise and lifting of the ice cover, possibly related to meltwater pulse (MWP) 1A (see text), allowed the meltwater to flowing underneath the ice and the accumulation of Unit 2 sediments. (C) The break-up of the ice cover produced big icebergs, which disturbed the sediment on top of Unit 2 on the topographic highs with their keels leaving widespread ploughmarks. (D) At a later phase of sea-level rise, ice melting favored the intense supply of suspended sediments leading to the accumulation of plumites intercalated by IRD layers (Unit 3). This material filled the ploughmarks. (E) The subsequent accumulation of Unit 4 sediments resulting from bottom currents probably occurred under iceberg-free conditions.

Fig. 10. Sequence stratigraphic interpretation of Units 1-4, based on PARASOUND profile 20130725_1752 (Fig. 3). Most of the succession are interpreted as part of the transgressive systems tract, bounded below by a glacial retreat surface, whereas highstand sediments possibly form the upper part of Unit 4.

Table 1. Radiocarbon dating.

Table 2. Acoustic units (Unit 1 to Unit 4 from the base to the top), defined from the PARASOUND profiles based on acoustic facies appearance. See text for details of the interpretation.

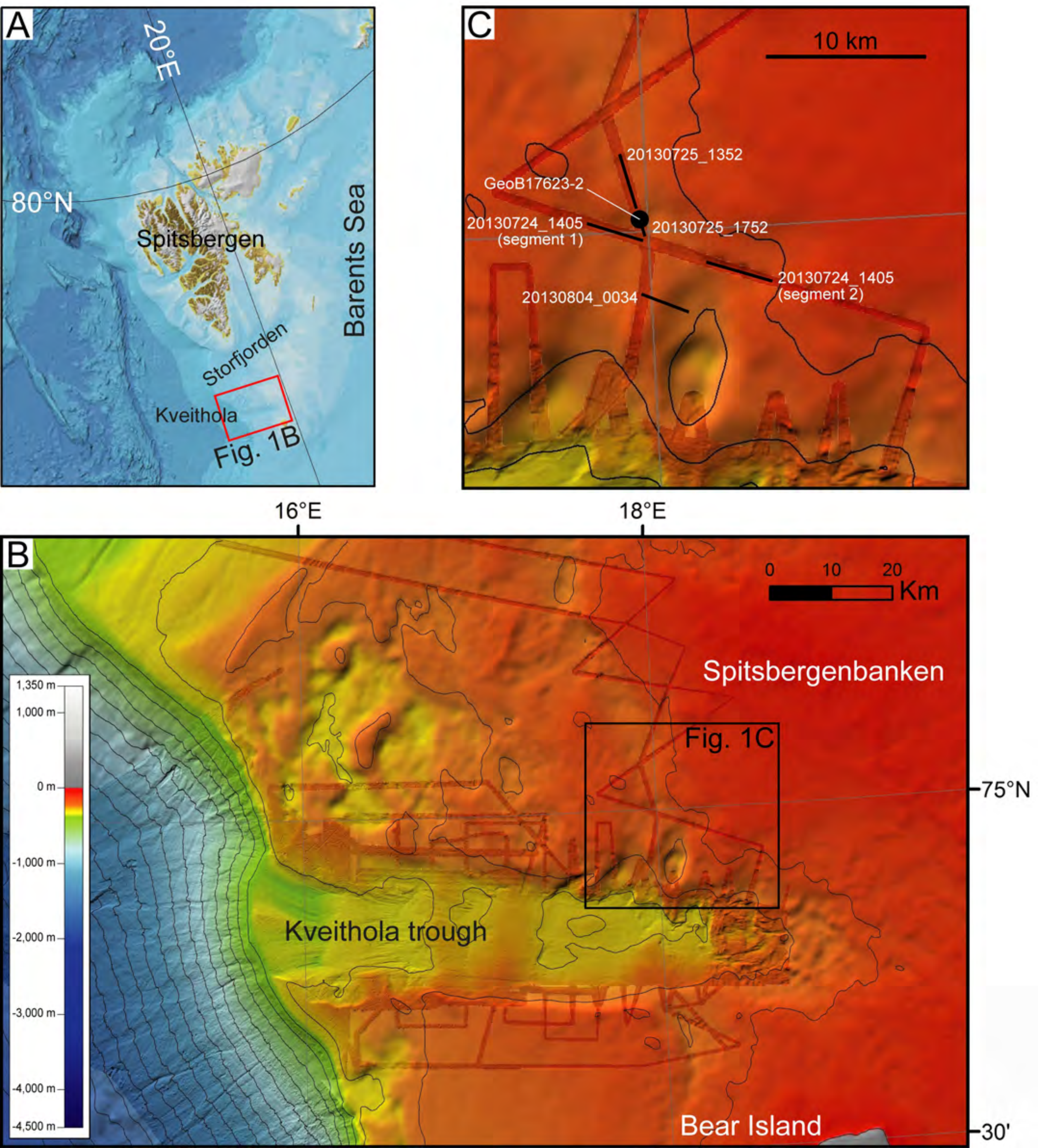

A
20°E
80°N
Spitsbergen
Barents Sea
Storfjorden
Kveithola
Fig. 1B
C
10 km
20130725_1352
GeoB17623-2
20130724_1405
(segment 1)
20130725_1752
20130724_1405
(segment 2)
20130804_0034
16°E
18°E
B
0
10
20
Km
Spitsbergenbanken
Fig. 1C
75°N
1,350 m
1,000 m
0 m
-1,000 m
-2,000 m
-3,000 m
-4,000 m
-4,500 m
Kveithola trough
Bear Island
30'

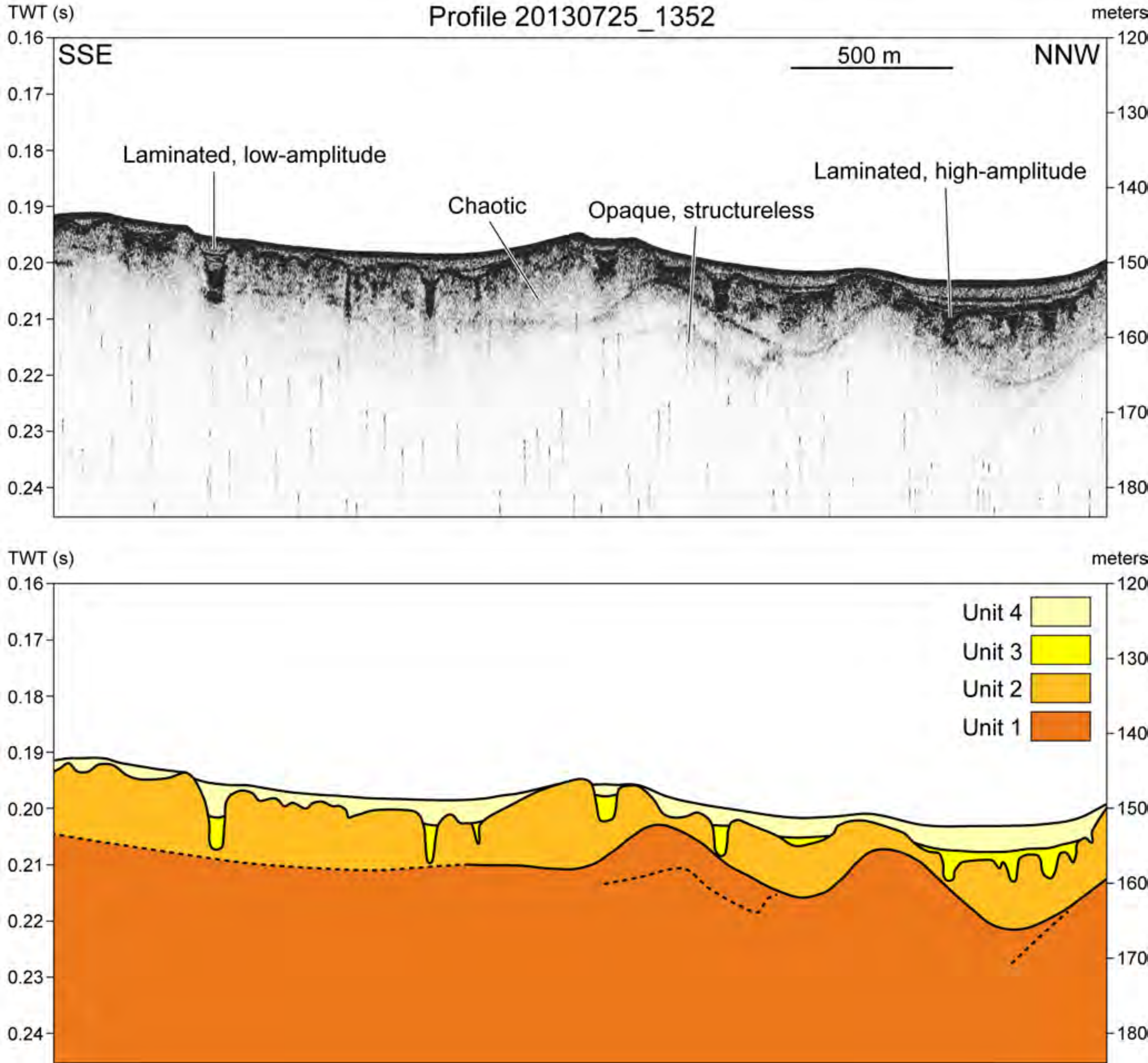
Profile 20130725_1352
TWT (s)
meters
SSE
NNW
500 m
Laminated, low-amplitude
Chaotic
Opaque, structureless
Laminated, high-amplitude
0.16
0.17
0.18
0.19
0.20
0.21
0.22
0.23
0.24
Unit 4
Unit 3
Unit 2
Unit 1

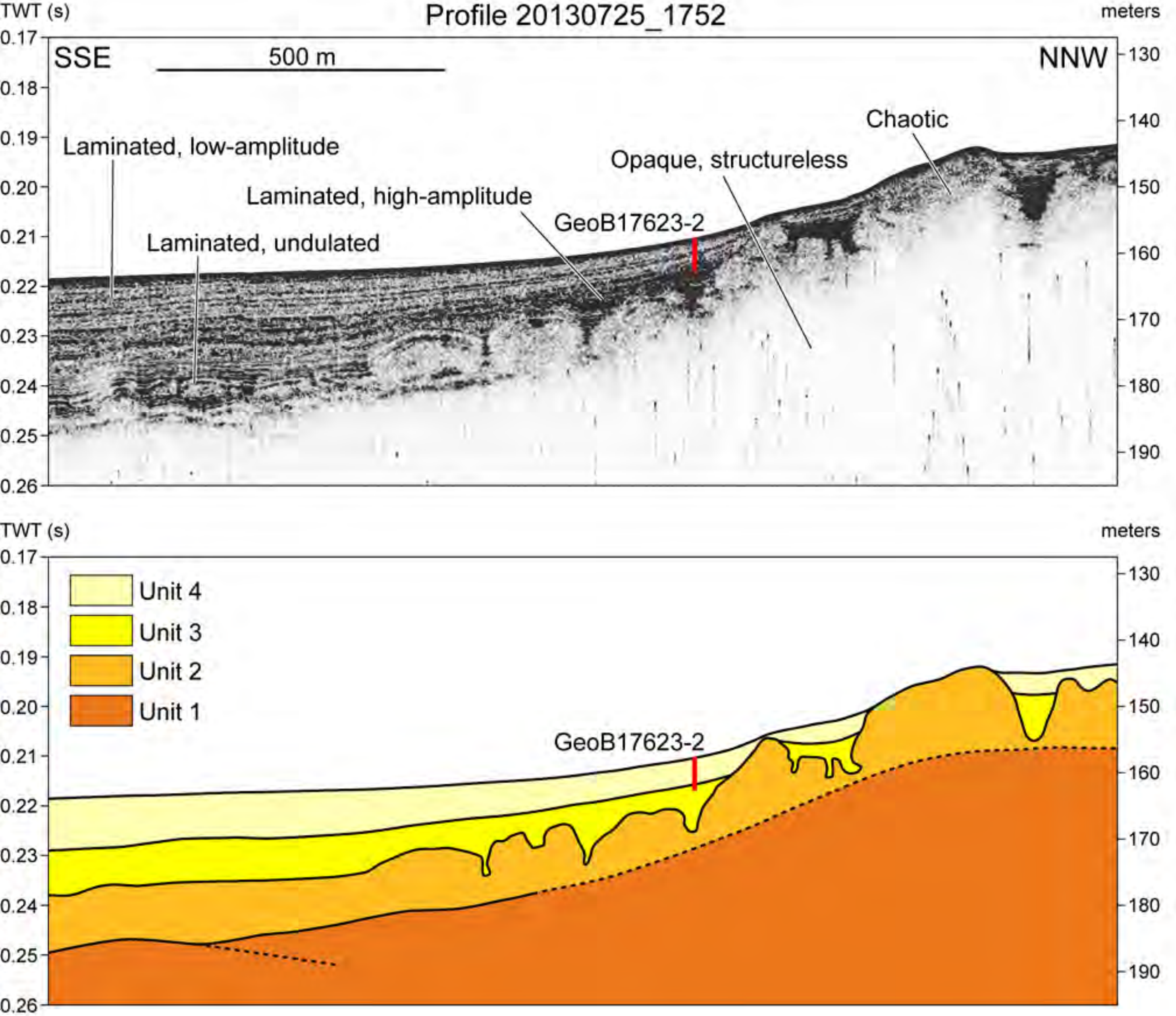

Profile 20130725_1752
TWT (s)
meters
SSE
500 m
NNW
Laminated, low-amplitude
Laminated, high-amplitude
Laminated, undulated
Opaque, structureless
Chaotic
GeoB17623-2
0.17
0.18
0.19
0.20
0.21
0.22
0.23
0.24
0.25
0.26
130
140
150
160
170
180
190
TWT (s)
meters
Unit 4
Unit 3
Unit 2
Unit 1
GeoB17623-2

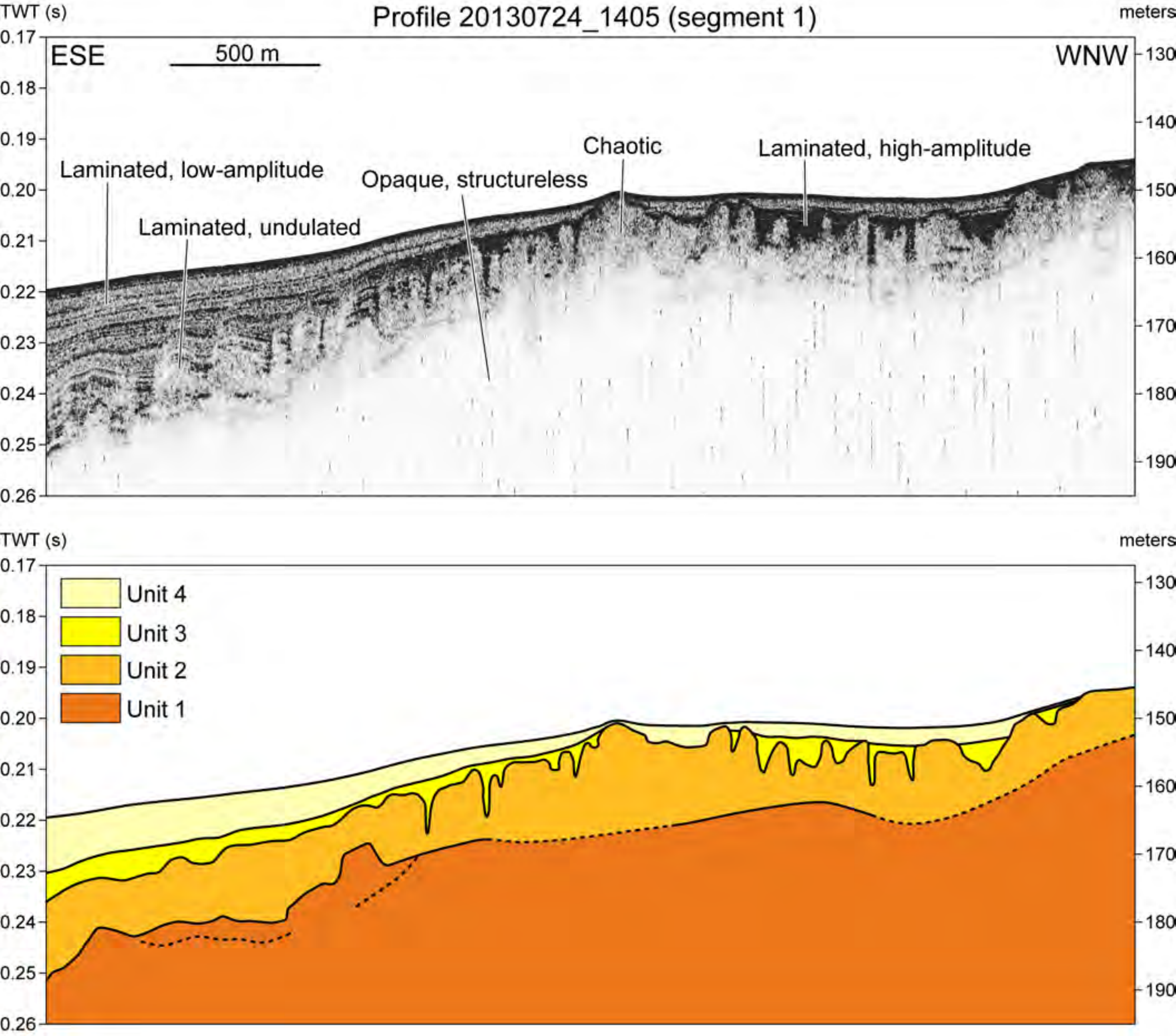

Profile 20130724_1405 (segment 1)
TWT (s)
meters
ESE
500 m
WNW
Laminated, low-amplitude
Laminated, undulated
Opaque, structureless
Chaotic
Laminated, high-amplitude
0.17
0.18
0.19
0.20
0.21
0.22
0.23
0.24
0.25
0.26
130
140
150
160
170
180
190
Unit 4
Unit 3
Unit 2
Unit 1

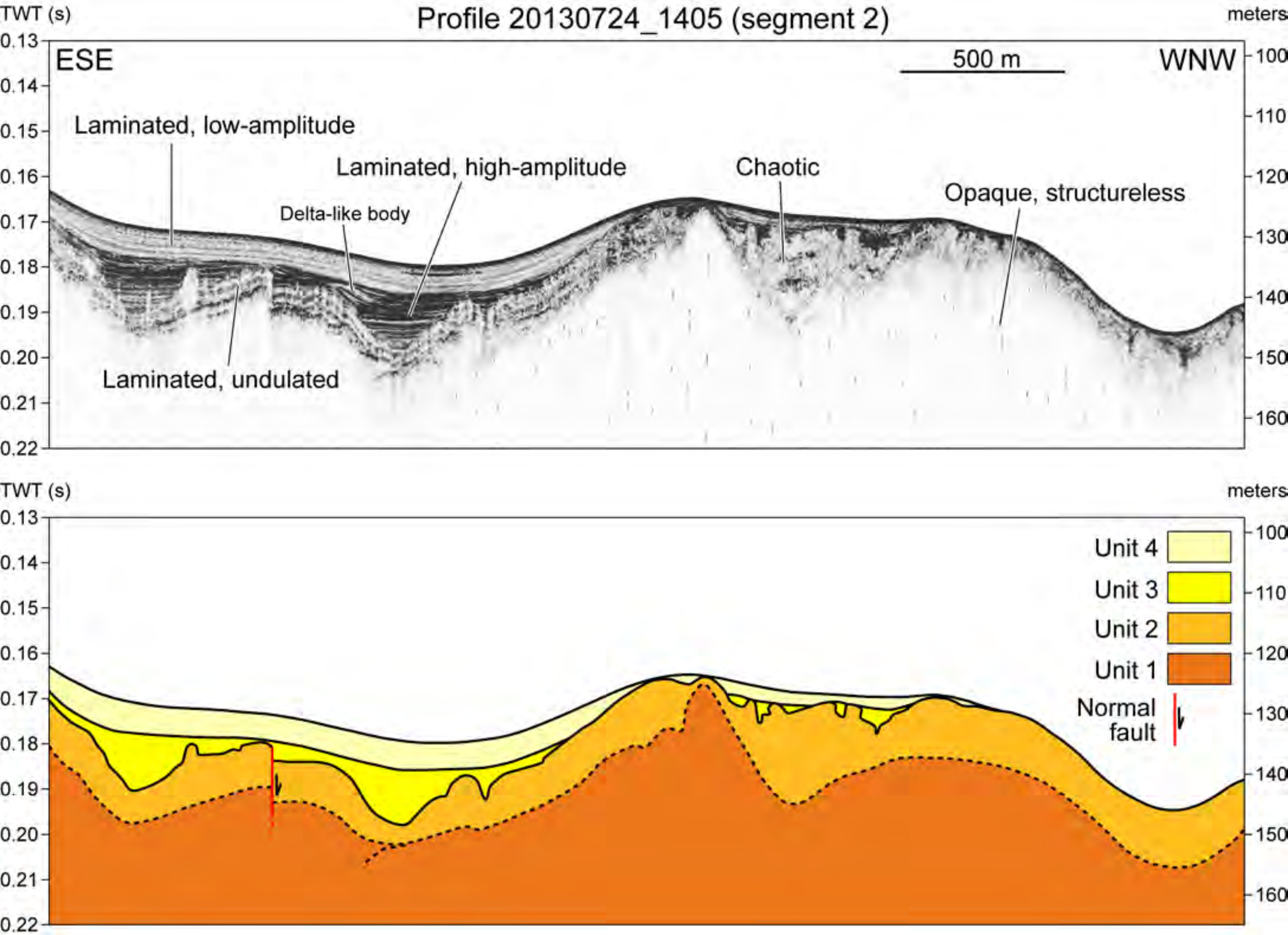
Profile 20130724_1405 (segment 2)
TWT (s)
meters
ESE
WNW
500 m
Laminated, low-amplitude
Laminated, high-amplitude
Chaotic
Opaque, structureless
Delta-like body
Laminated, undulated
0.13
0.14
0.15
0.16
0.17
0.18
0.19
0.20
0.21
0.22
Unit 4
Unit 3
Unit 2
Unit 1
Normal fault

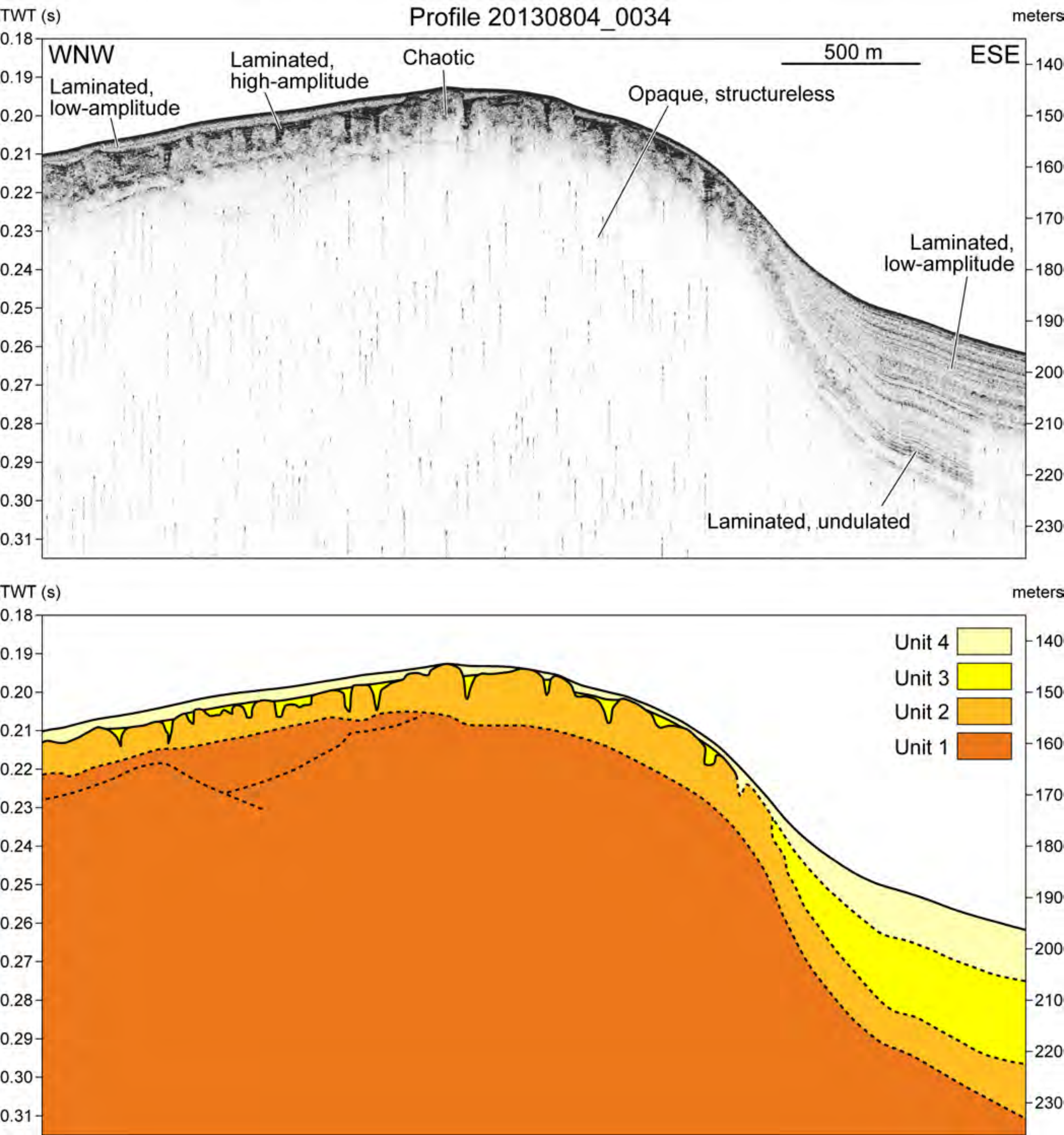

Profile 20130804_0034
TWT (s)
meters
WNW
ESE
500 m
Laminated, low-amplitude
Laminated, high-amplitude
Chaotic
Opaque, structureless
Laminated, low-amplitude
Laminated, undulated
0.18
0.19
0.20
0.21
0.22
0.23
0.24
0.25
0.26
0.27
0.28
0.29
0.30
0.31
140
150
160
170
180
190
200
210
220
230
TWT (s)
meters
Unit 4
Unit 3
Unit 2
Unit 1

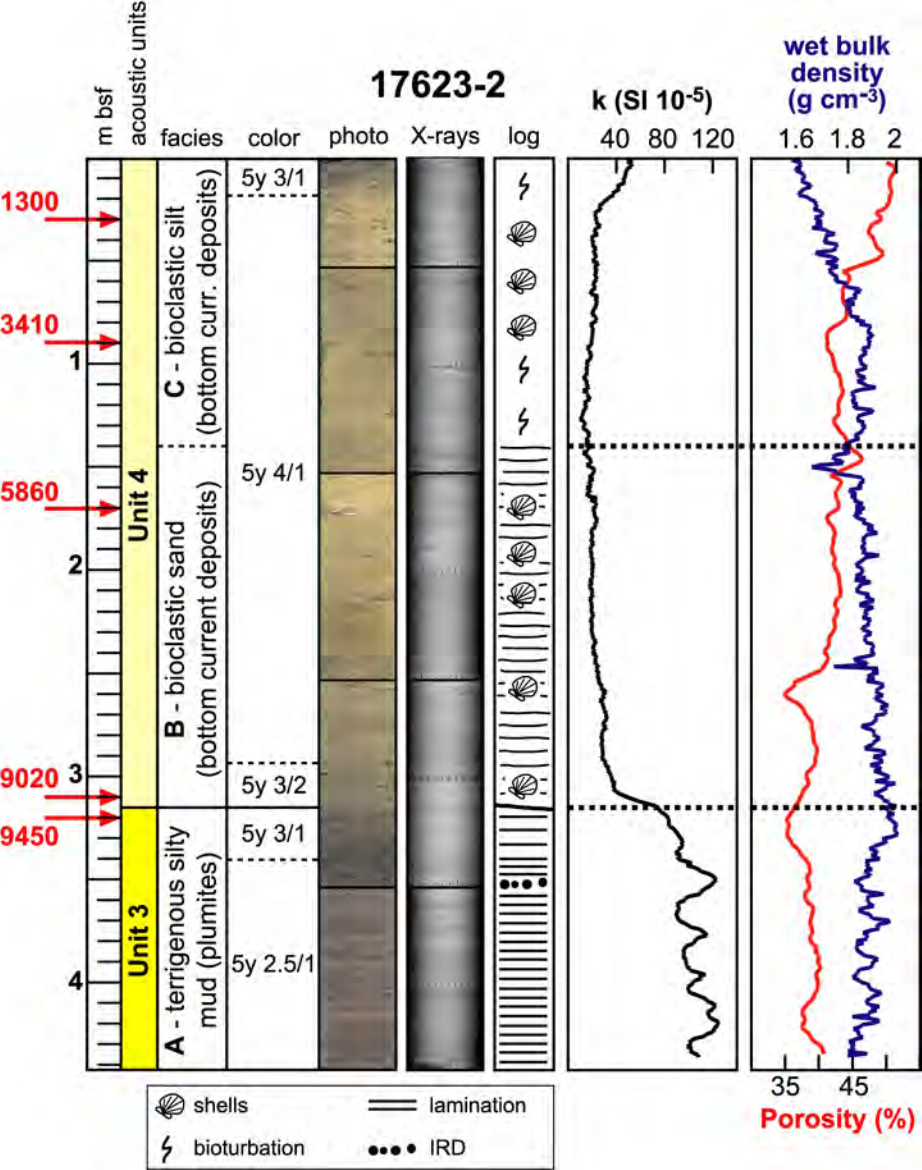

17623-2
m bsf
acoustic units
facies
color
photo
X-rays
log
k (SI 10-5)
40 80 120
wet bulk density (g cm-3)
1.6 1.8 2
1300
3410
5860
9020
9450
1
2
3
4
Unit 4
Unit 3
C - bioclastic silt (bottom curr. deposits)
B - bioclastic sand (bottom current deposits)
A - terrigenous silty mud (plumites)
5y 3/1
5y 4/1
5y 3/2
5y 3/1
5y 2.5/1
35 45
Porosity (%)
shells
bioturbation
lamination
IRD

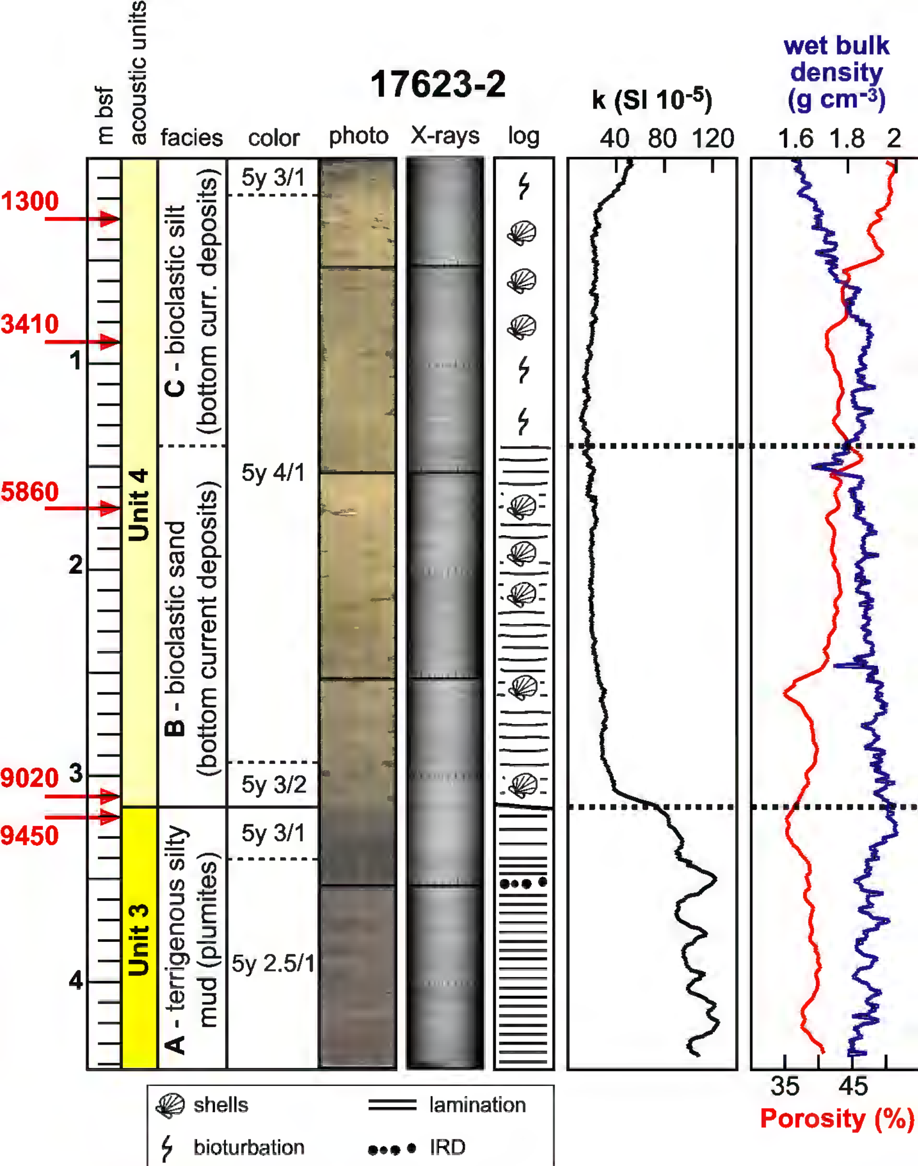

17623-2
m bsf
acoustic units
facies
color
photo
X-rays
log
k (SI 10-5)
40
80
120
wet bulk density (g cm-3)
1.6
1.8
2
1300
3410
5860
9020
9450
1
2
3
4
Unit 4
Unit 3
C - bioclastic silt (bottom curr. deposits)
B - bioclastic sand (bottom current deposits)
A - terrigenous silty mud (plumites)
5y 3/1
5y 4/1
5y 3/2
5y 3/1
5y 2.5/1
35
45
Porosity (%)
shells
bioturbation
lamination
IRD

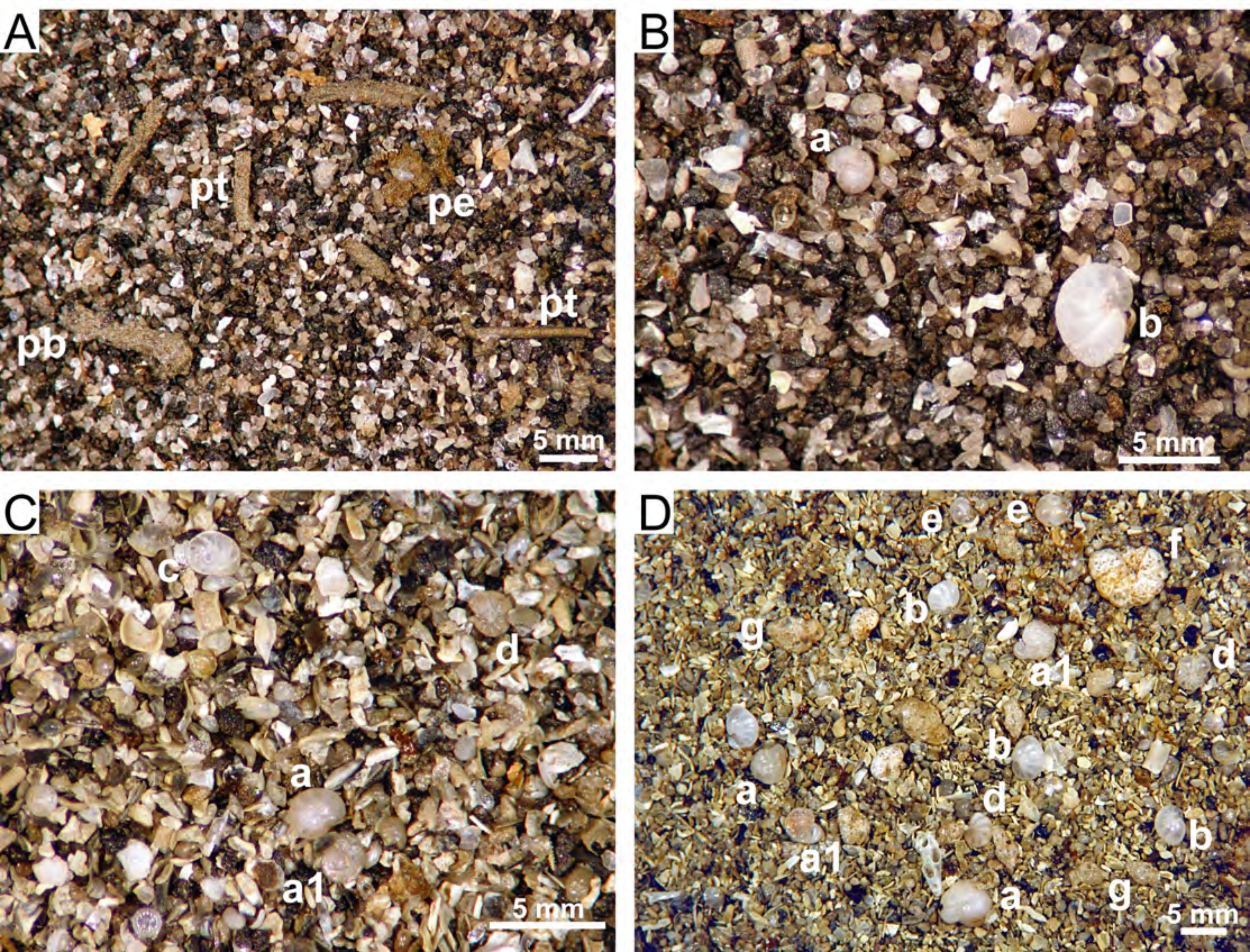
A
pt
pe
pt
pb
5 mm
B
a
b
5 mm
C
c
d
a
a1
5 mm
D
e
e
f
b
g
a1
d
b
a
d
b
a1
a
g
5 mm

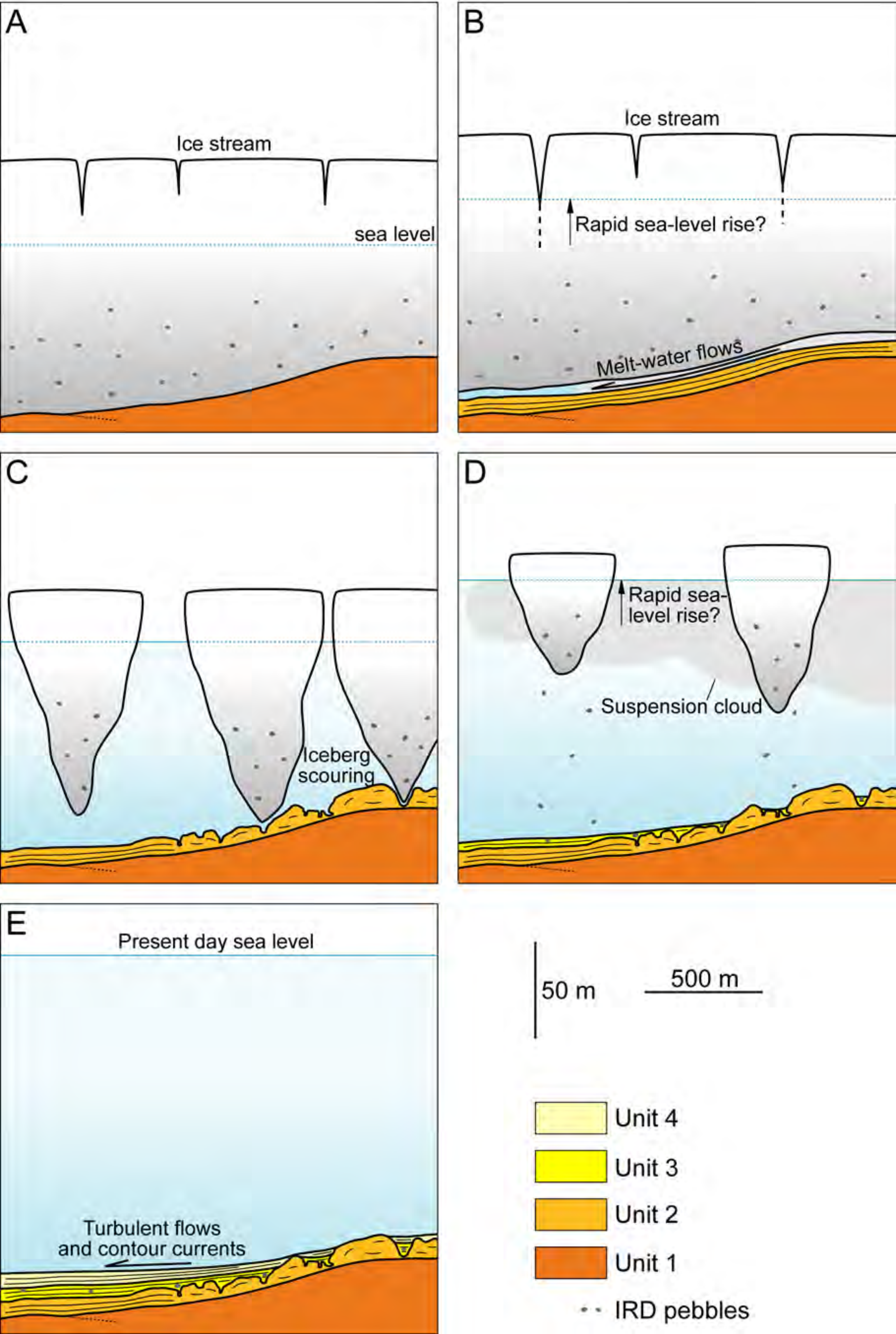
A
Ice stream
sea level
B
Ice stream
Rapid sea-level rise?
Melt-water flows
C
Iceberg scouring
D
Rapid sea-level rise?
Suspension cloud
E
Present day sea level
Turbulent flows and contour currents
50 m
500 m
Unit 4
Unit 3
Unit 2
Unit 1
IRD pebbles

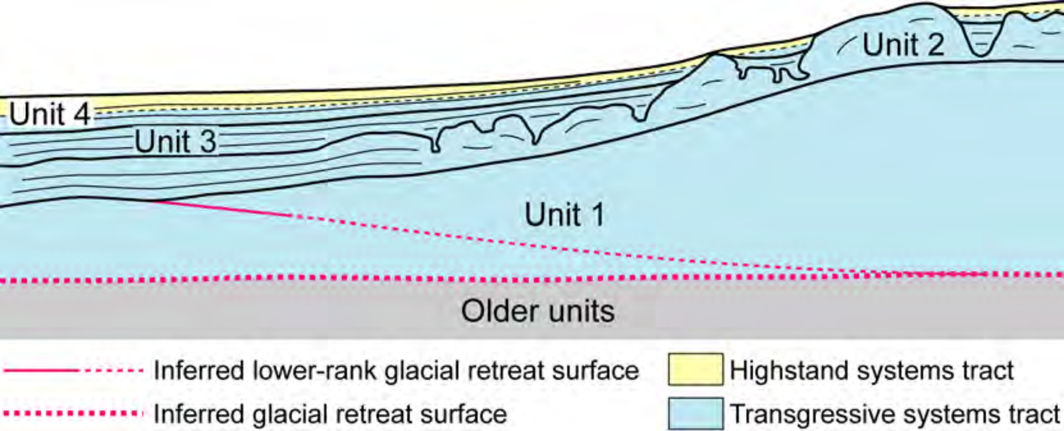
Unit 2
Unit 4
Unit 3
Unit 1
Older units
Inferred lower-rank glacial retreat surface
Inferred glacial retreat surface
Highstand systems tract
Transgressive systems tract